Tunable Backaction of a DC SQUID on an Integrated Micromechanical Resonator

M. Poot,[1,*] S. Etaki,[1,2] I. Mahboob,[2] K. Onomitsu,[2] H. Yamaguchi,[2] Ya. M. Blanter,[1] and H. S. J. van der Zant[1,†]

[1]*Kavli Institute of Nanoscience, Delft University of Technology, Post Office Box 5046, 2600 GA Delft, Netherlands*

[2]*NTT Basic Research Laboratories, NTT Corporation, Atsugi-shi, Kanagawa 243-0198, Japan*

(Received 4 May 2010; published 10 November 2010)

We have measured the backaction of a dc superconducting quantum interference device (SQUID) position detector on an integrated 1 MHz flexural resonator. The frequency and quality factor of the micromechanical resonator can be tuned with bias current and applied magnetic flux. The backaction is caused by the Lorentz force due to the change in circulating current when the resonator displaces. The experimental features are reproduced by numerical calculations using the resistively and capacitively shunted junction model.

DOI: 10.1103/PhysRevLett.105.207203 PACS numbers: 85.85.+j, 05.45.−a, 46.40.Ff, 85.25.Dq

It has recently been demonstrated that a macroscopic mechanical resonator can be put in a quantum state [1] by coupling it to another quantum system. At the same time, linear detectors coupled to mechanical resonators are rapidly approaching the quantum limit on position detection. This limit implies that the resonator position cannot be measured with arbitrary accuracy, as the detector itself affects the resonator position [2]. This is an example of backaction. Backaction does not just impose limits, it can also work to one's advantage: Backaction can cool the resonator, squeeze its motion, and couple and synchronize multiple resonators. Different backaction mechanisms have been identified: When using optical interferometers [3–6] or electronic resonant circuits [7–9], backaction results from radiation pressure. In single-electron transistors [10], Cooper-pair boxes [11], carbon nanotube quantum dots [12,13], or atomic and quantum point contacts [14,15] backaction is due to the tunneling of electrons. Recently, we have used a dc SQUID as a sensitive detector of the position of an integrated mechanical resonator [16]. This embedded resonator-SQUID geometry enables the experimental realization of a growing number of theoretical proposals for which a good understanding of the backaction is required [17–23].

In this Letter, we present experiments that show that the dc SQUID detector exerts backaction on the resonator. By adjusting the bias conditions of the dc SQUID the frequency and damping of the mechanical resonator change. The backaction by the dc SQUID has a different origin than in the experiments mentioned above: It is due to the Lorentz force generated by the circulating current. Numerical calculations using the resistively and capacitively shunted junction model for the dc SQUID [24] reproduce the experimental features.

The device [Fig. 1(a)] consists of a dc SQUID with proximity-effect-based junctions [16]. A part of one arm is underetched, forming a 1 MHz flexural resonator with length $\ell = 50\ \mu$m. In this Letter we present data on a device in an in-plane magnetic field of $B = 100$ mT. Measurements have been performed at several magnetic fields and on an additional device; the observed backaction is similar [25]. First the dc SQUID is characterized. The output voltage of a dc SQUID depends on the magnetic flux through its loop Φ [24] and we measure the minimum and maximum voltage ($V_{\min}$ and $V_{\max}$) by sweeping the flux over a few flux quanta $\Phi_0 = h/2e$ with a nearby stripline [Fig. 1(a)]. This is repeated for different bias currents to obtain the current-voltage curves shown in Fig. 1(b). The maximum critical current is $I_c^{\max} = 2.19\ \mu$A and the normal-state resistance of the junctions is $R = 15.6\ \Omega$. After this characterization, the dc SQUID

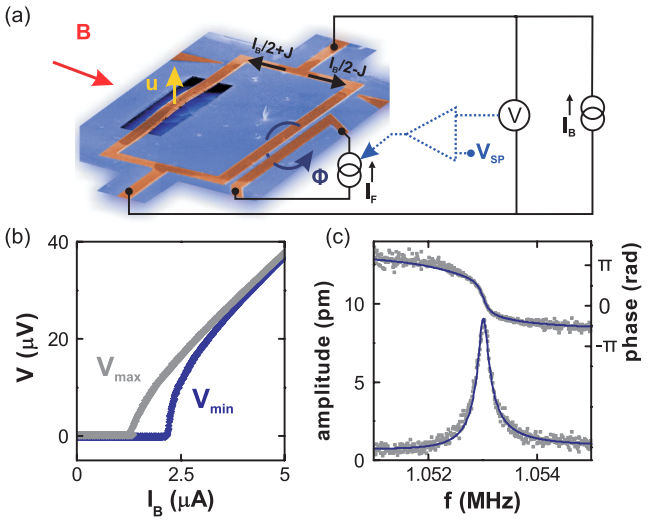

FIG. 1 (color online). (a) Schematic overview of the dc SQUID with the suspended beam and measurement setup. A magnetic field B transduces a beam displacement u into a change in magnetic flux. A bias current I_B is sent through the SQUID and its output voltage is measured. The flux Φ is fine-tuned with a stripline current I_F that is controlled by a feedback circuit (dashed) that keeps the output voltage V at V_{SP}. (b) The bias current dependence of the measured $V_{\min}$ and $V_{\max}$. (c) The amplitude (bottom) and phase (top) response. The line is a fitted harmonic oscillator response [33].

is operated at a given setpoint voltage V_{SP} using a feedback loop that adjusts the flux via the stripline current [16,24]. The feedback loop is used to reduce low-frequency flux noise and flux drift and has a bandwidth of $\sim$2 kHz; i.e., it does not respond to the 1 MHz resonator signal.

The fundamental mode of the flexural resonator is excited using a piezo element underneath the sample and the displacement of the beam is detected as follows: The in-plane magnetic field transduces a displacement of the beam u into a flux change $\sim \ell B u$, which in turn changes the voltage over the dc SQUID. This voltage is amplified using a cryogenic high-electron mobility transistor followed by a room temperature amplifier and then recorded using a network analyzer. Figure 1(c) shows the amplitude and phase of the measured response, from which the resonance frequency f_R and quality factor Q are obtained.

To observe backaction of the dc SQUID detector on the resonator, the frequency response is measured for different bias conditions of the SQUID. Figure 2 shows that both f_R and Q depend on the bias current I_B. The resonance frequency saturates at $f_0 = 1.053\,010$ MHz for large positive and negative bias currents. However, when decreasing the I_B, f_R first goes up by a few hundred Hz around $I_c^{\max}$ and then it decreases rapidly with about -2000 Hz at the lowest stable setpoint voltage. This is more than $10\times$ the linewidth $f_R/Q = 194$ Hz of the resonance shown in Fig. 1(c). Figure 2(b) shows that the quality factor of the resonator changes from $Q_0 = 5300$ to less than 2000. Similar to the resonance frequency, first an increase and then a stronger decrease in Q is observed when lowering the bias current. Figure 3 shows that the frequency and damping can also be changed by adjusting V_{SP}, i.e., the flux through the SQUID loop. The shifts are largest for low setpoints and low bias currents (dark regions). The regions with a lower frequency coincide with the regions where the damping has increased. Bias points with positive frequency shifts and increases in Q are indicated in white. Finally, by varying the driving power we confirm that the observed effects are not due to nonlinearities in the SQUID or in the resonator [25].

Unlike for position detectors such as the single-electron transistors where the backaction originates from the Coulomb force, the backward coupling between the SQUID and the beam is the Lorentz force F_L [18,21]. This force is due to the current that flows through the beam in the presence of the magnetic field that couples the resonator and the SQUID. A displacement changes the flux, and this in turn changes the circulating current in the loop J [24], giving a different force on the beam. In addition, resonator motion yields a time-varying flux through the loop, which induces an electromotive force and thereby also generates currents that change the Lorentz force [26].

The displacement of the fundamental out-of-plane flexural mode u is given by [27]

$$m\ddot{u} + m\omega_0\dot{u}/Q_0 + m\omega_0^2 u = F_d(t) + F_L(t). \qquad (1)$$

The resonator has a mass m, (intrinsic) frequency $f_0 = \omega_0/2\pi$ and quality factor Q_0. F_d is the driving force and $F_L = aB\ell(I_B/2 + J)$ is the Lorentz force. Here, $a = (u\ell)^{-1}\int_0^\ell u(x)dx \approx 0.9$ for the fundamental mode, so that also $\partial\Phi/\partial u = aB\ell$ [16,27]. For small amplitudes and low resonator frequencies (much smaller than the characteristic SQUID frequency $\omega_c = \pi R I_c^{\max}/\Phi_0$), the average circulating current can be expanded in the displacement and velocity $\dot{u}$ [25]:

$$J(u,\dot{u}) = J_0 + \frac{\partial J}{\partial \Phi} aB\ell u + \frac{\partial J}{\partial \dot{\Phi}} aB\ell \dot{u}. \qquad (2)$$

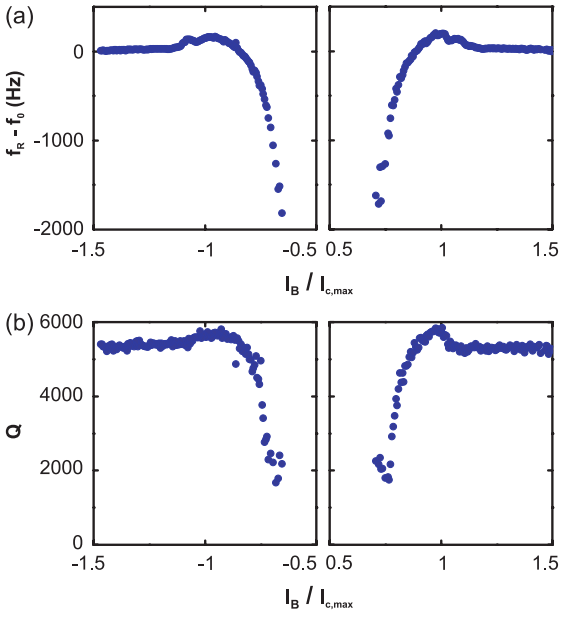

FIG. 2 (color online). Frequency shift (a) and quality factor (b) plotted versus the normalized bias current. The voltage setpoint was halfway between $V_{\min}$ and $V_{\max}$ in these measurements.

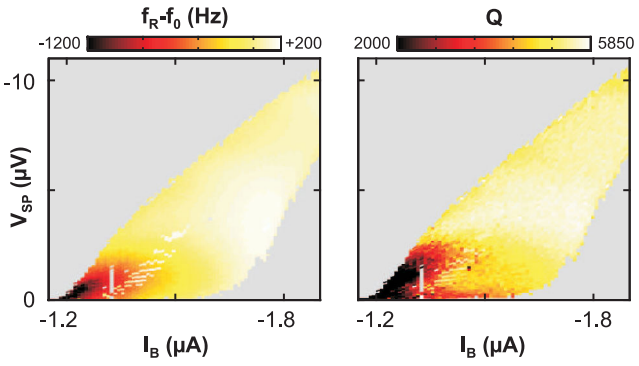

FIG. 3 (color online). Measured bias current and voltage setpoint dependence of the frequency shift (left panel) and damping (right panel). Points without a good lock are indicated in gray.

Inserting Eq. (2) into Eq. (1) shows that the $\partial J/\partial\Phi$ term affects the spring constant $m\omega_R^2$ and thus f_R, whereas the $\partial J/\partial\dot{\Phi}$ term renormalizes the damping. The shifted resonance frequency and quality factor are

$$f_R = f_0(1 - \Delta_f J_\phi)^{1/2}, \quad \text{with} \quad \Delta_f = \frac{a^2B^2\ell^2}{m\omega_0^2}\frac{I_c^{\max}}{2\Phi_0}, \quad (3)$$

$$Q = Q_0\frac{f_R}{f_0}\frac{1}{1 - \Delta_Q J_{\dot{\phi}}}, \quad \text{with} \quad \Delta_Q = \frac{a^2B^2\ell^2}{m\omega_0 R}\frac{Q_0}{2\pi}. \quad (4)$$

Here, $J_\phi = \partial J/\partial\Phi \times 2\Phi_0/I_c^{\max}$ and $J_{\dot{\phi}} = \partial J/\partial\dot{\Phi} \times 2\omega_c\Phi_0/I_c^{\max}$ are the scaled flux-to-current transfer functions [28]. The former indicates how much the circulating current changes when the flux through the ring is altered, whereas the latter quantifies the effect of a time-dependent flux on the circulating current. These functions were first studied in the analysis of the dynamic input impedance of tuned SQUID amplifiers [28,29] and are intrinsic properties of the SQUID.

Before looking in more detail at the transfer functions, we first focus on the coupling. The dimensionless parameters Δ_f [20] and Δ_Q characterize the backaction strength. They contain the term $aB\ell$ squared as both the flux change and the Lorentz force are proportional to the magnetic field. This implies that the backaction remains the same when the direction of the magnetic field is reversed and this is what we observe experimentally. Δ_f is proportional to $I_c^{\max}$, whereas the damping induced by the SQUID depends on R. By a careful design of the resonator and SQUID, the backaction strengths can be tuned over a wide range. Equations (3) and (4) show that the largest backaction occurs for large flux changes $aB\ell$, low spring constants $m\omega_0^2$, and large circulating currents, i.e., large $I_0 = I_c^{\max}/2$ and low R. For the device studied in this Letter, we estimate $\Delta_f = 4.1 \times 10^{-4}$ and $\Delta_Q = 2.8 \times 10^{-4}$. Finally, note that the two coupling parameters are related by $\Delta_Q = \Delta_f \times Q_0\omega_0/\omega_c$.

So far, the analysis did not assume anything about the number of junctions, nor about their microscopic details. To obtain the transfer functions J_ϕ and $J_{\dot{\phi}}$, we model the junctions in the dc SQUID using the resistively and capacitively shunted junction model [24]. The transfer functions can be calculated analytically in certain limits [30]. However, to obtain their full bias-condition dependence, J_ϕ and $J_{\dot{\phi}}$ must be calculated numerically. This is done by simulating the dynamics of the SQUID in the presence of a time-varying flux [25]. Figure 4(a) shows the bias dependence of J_ϕ. In the region where $V = 0$, the circulating current redistributes the bias current between the two junctions such that no voltage develops. Here the circulating current is of the order of $I_c^{\max}/2$, which gives $J_\phi \sim -1$ (blue). In the dissipative region ($V \neq 0$), the circulating current is suppressed. Therefore, the circulating current changes rapidly close to the edge of the dissipative region. The orange color in Fig. 4(a) indicates that J_ϕ is large and positive near the critical current. The largest downward frequency shift is expected near a half-integer number of flux quanta, whereas J_ϕ vanishes for integer flux. With the value of the coupling parameter Δ_f and the resonance frequency f_0 the frequency shift is calculated as shown in Fig. 4(c). The maximum value $J_\phi = 53$ gives a frequency shift of -12 kHz in the lower-left corner, which has to be compared with the experimental value of ~ -2 kHz. Increasing the bias current above the critical current results in a smaller J_ϕ (light yellow and light blue) that depends linearly on the inductive screening parameter β_L [24] for the experimental conditions. In this region the simulations predict both positive (blue) and negative (yellow) value for J_ϕ. Positive and negative shifts are also observed in the experiment [Figs. 2 and 3]. The largest negative value found in the simulations of that region is $J_\phi = -0.65$, which results in an increase in f_R of $\sim$140 Hz, which is in agreement with the observed value of $\sim$200 Hz [Fig. 2(a)]. For even larger bias currents, the frequency shift vanishes: $f_R \approx f_0$. This corresponds to the flat regions in Fig. 2(a).

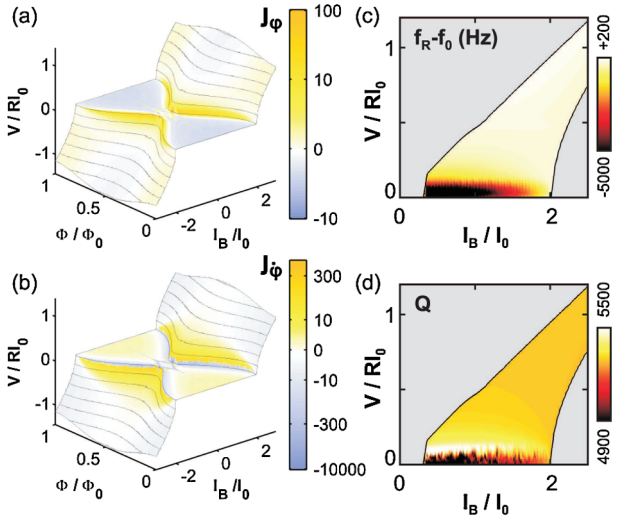

FIG. 4 (color online). Surface plots with isovoltage lines at different bias conditions of a dc SQUID. The (logarithmic) color scale represents the calculated flux-to-current transfer functions J_ϕ (a) and $J_{\dot{\phi}}$ (b). With the values for Δ_f and Δ_Q, the frequency shift (c) and quality factor change (d) are calculated. The simulation is done for the experimental conditions where the inductive screening parameter $\beta_L = 0.21$ and the Stewart-McCumber parameter $\beta_C = 0.23$ [24,25].

The change in damping is determined by $J_{\dot{\phi}}$ as indicated by Eq. (4). Its dependence on the bias conditions is shown in Fig. 4(b). Well inside the experimentally inaccessible nondissipative region $J_{\dot{\phi}} \sim +1$ and the backaction results in a small increase in Q. In the opposite limit of large bias

currents $J_\phi = -\pi$ (light blue). This value combined with the small value of Δ_Q implies that the quality factor in the flat region in Fig. 2(b) is close to the intrinsic Q factor, Q_0. In this region the small additional damping is due to the current induced by the time-varying flux $\dot{\Phi}/2R$, which is dissipated in the junction resistances [30]. This contribution is well known from magnetomotive readout of mechanical resonators [26]. When lowering the bias current, J_ϕ changes sign and rises to about +500. This reduces the damping and might even lead to instability ($Q < 0$) if Δ_Q is large enough. This decrease of damping corresponds to the bumps in Fig. 2(b). The largest observed quality factor $Q = 5800$ corresponds to $J_\phi = +400$, which is in reasonable agreement with the simulations. Close to the critical current, J_ϕ goes to large *negative* values leading to an enhanced dissipation. Figure 4(d) shows that the calculated Q factor is indeed lowest near the critical current. In summary, our model shows that although the coupling strength is small, the dynamics of the dc SQUID greatly enhances the backaction.

Various interesting effects can be observed when the backaction is strong. If the resonator and SQUID are strongly coupled, the resonator temperature is set by the effective bath temperature [10,14] of the SQUID. The increased damping cools the resonator, but the shot noise in the bias current leads to an increase in the force noise on the resonator, heating it. The question whether the resonator temperature is above or below the environmental temperature should be addressed in future research. Furthermore, the dependence of f_R and Q on the bias conditions allows parametric excitation of the mechanical resonator by either modulating the flux or the bias current. This enables squeezing of the thermomechanical noise of the resonator [20,31]. Finally, if the SQUID contains multiple, nearly identical mechanical resonators, these are coupled to each other by the backaction. This, in turn, can synchronize their motion and might lead to frequency entrainment if higher order terms in Eq. (2) become significant [32]. These examples are only a few intriguing possibilities of the rich physics connected to the backaction that we have described in this Letter.

We thank T. Akazaki, H. Okamoto, and K. Yamazaki for help with fabrication and R. Schouten for the measurement electronics. This work was supported in part by JSPS KAKENHI (20246064 and 18201018), FOM, NWO (VICI grant), and a EU FP7 STREP project (QNEMS).

*menno.poot@yale.edu
†h.s.j.vanderzant@tudelft.nl

[1] A. D. O'Connell *et al.*, Nature (London) **464**, 697 (2010).
[2] C. M. Caves *et al.*, Rev. Mod. Phys. **52**, 341 (1980).
[3] S. Gigan *et al.*, Nature (London) **444**, 67 (2006).
[4] O. Arcizet *et al.*, Nature (London) **444**, 71 (2006).
[5] J. D. Thompson *et al.*, Nature (London) **452**, 72 (2008).
[6] G. Anetsberger *et al.*, Nature Phys. **5**, 909 (2009).
[7] J. D. Teufel *et al.*, Phys. Rev. Lett. **101**, 197203 (2008).
[8] K. R. Brown *et al.*, Phys. Rev. Lett. **99**, 137205 (2007).
[9] T. Rocheleau *et al.*, Nature (London) **463**, 72 (2010).
[10] A. Naik *et al.*, Nature (London) **443**, 193 (2006).
[11] M. D. LaHaye *et al.*, Nature (London) **459**, 960 (2009).
[12] G. A. Steele *et al.*, Science **325**, 1103 (2009).
[13] B. Lassagne *et al.*, Science **325**, 1107 (2009).
[14] N. E. Flowers-Jacobs, D. R. Schmidt, and K. W. Lehnert, Phys. Rev. Lett. **98**, 096804 (2007).
[15] J. Stettenheim *et al.*, Nature (London) **466**, 86 (2010).
[16] S. Etaki *et al.*, Nature Phys. **4**, 785 (2008).
[17] X. Zhou and A. Mizel, Phys. Rev. Lett. **97**, 267201 (2006).
[18] M. P. Blencowe and E. Buks, Phys. Rev. B **76**, 014511 (2007).
[19] F. Xue *et al.*, Phys. Rev. B **76**, 064305 (2007).
[20] W. Y. Huo and G. L. Long, Appl. Phys. Lett. **92**, 133102 (2008).
[21] P. D. Nation, M. P. Blencowe, and E. Buks, Phys. Rev. B **78**, 104516 (2008).
[22] E. Buks and M. P. Blencowe, Phys. Rev. B **74**, 174504 (2006).
[23] F. Xue *et al.*, New J. Phys. **9**, 35 (2007).
[24] J. Clarke and A. Braginski, *The SQUID Handbook* (Wiley-VCH, Verlag, GmbH and Co. KGaA, Weinheim, 2004), Vol. 1.
[25] See supplementary materials at http://link.aps.org/supplemental/10.1103/PhysRevLett.105.207203.
[26] A. N. Cleland and M. L. Roukes, Sens. Actuators A, Phys. **72**, 256 (1999).
[27] A. N. Cleland and M. L. Roukes, J. Appl. Phys. **92**, 2758 (2002).
[28] C. Hilbert and J. Clarke, J. Low Temp. Phys. **61**, 237 (1985).
[29] P. Falferi *et al.*, Appl. Phys. Lett. **71**, 956 (1997).
[30] Ya. M. Blanter (to be published).
[31] D. Rugar and P. Grütter, Phys. Rev. Lett. **67**, 699 (1991).
[32] S.-B. Shim, M. Imboden, and P. Mohanty, Science **316**, 95 (2007).
[33] Our fits take into account the small crosstalk between the driving signal and output voltage that is present in the experiment. This effect makes the line shape slightly asymmetric.